



Ultra-low reflection CuO nanowire array in-situ grown on copper sheet



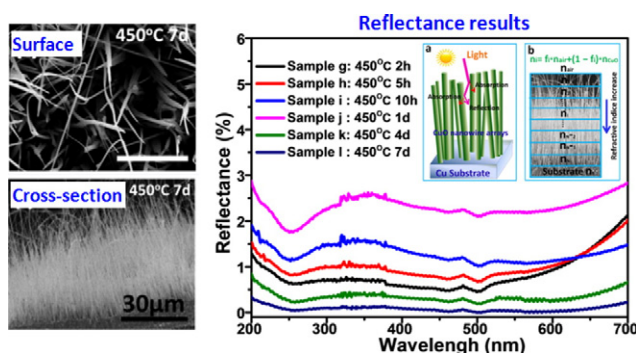
Xingli Wang, Xiaofeng Wu, Long Yuan, Keke Huang, Shouhua Feng*

State Key Laboratory of Inorganic Synthesis and Preparative Chemistry, College of Chemistry, Jilin University, Changchun 130012, PR China

HIGHLIGHTS

- CuO nanowires were orderly grown on Cu sheet, which show ultra-low reflection with the reflectance of 0.078% in 200–700 nm.
- The low reflection of CuO nanowires can be attributed to multiple reflection and absorption of incident light.
- These materials can be applied in improving the absorption of the inner-wall of sensitive optical instruments.

GRAPHICAL ABSTRACT



The ultra-low reflection CuO/Cu material in UV–vis range is successfully designed and achieved, via orderly growing ultralong CuO nanowires to construct the thick and vertically aligned array. The blackest sample obtains an ultra-low reflectance of 0.078% in 200–700 nm region. The preparation method of the above ultra-low reflection material is suitable for industrial production.

ARTICLE INFO

Article history:

Received 12 July 2016

Received in revised form 28 September 2016

Accepted 14 October 2016

Available online 17 October 2016

Keywords:

Ultra-low reflectance materials

Vertically aligned

Light trapping

Solar energy harvesting

Optical instruments

ABSTRACT

Ultra-low reflectance materials are widely applied in the solar energy harvesting, the space instruments, spectrometers and terrestrial telescopes. The ultra-low reflection material of CuO/Cu in UV–vis is designed and achieved via orderly growing ultralong CuO nanowires on copper sheet, constructing the ultra-thick and vertically aligned array. The reflectance of the resultant samples range from 0.078% to 5.31%, via controlling the thickness and density of CuO nanowire arrays at different growth temperature and time. Among them, the blackest sample obtains an ultra-low reflectance of 0.078% in 200–700 nm region and 0.0235% within the 500 nm–600 nm range. The ultra-low reflectivity of CuO nanowire arrays come from the following reasons: 1. the array is so thick and dense that the light can be multiply reflected and absorbed while propagates deep into the interspace of the nanowires, leading to an excellent light trapping. 2. The array can be regarded as air-filled gradient refractive index medium, which is also in favor of the low reflection. The CuO nanowire array represents a new-family of ultra-low reflection material in UV–vis. It will improve the sensitivity of optical instruments efficiently by blackening the inner-wall of drawtube or sample compartment for reducing stray light.

© 2016 Elsevier Ltd. All rights reserved.

1. Introduction

The ultra-low reflection materials are valuable in many applications. A good choice is for solar energy collector efficiently converting light to heat [1,2]. As these materials almost have no light reflection and astigmatism and contribute to blackening the inner-wall of drawtube or

* Corresponding author.

E-mail address: shfeng@jlu.edu.cn (S. Feng).

sample compartment, therefore it is potential to improve the detect ability of infrared optical systems [3–5], increase the sensitivity of astronomical telescope, and calibrate the astronomical camera.

Recently, many nanostructures were designed to increase the multiple reflection (or absorption) and obtain the low-reflection by different ways such as chemical treatment (nickel-phosphorus black surfaces) [6], spin-casting (nanoporous latex film) [7], electrochemistry (black nickel-cobalt plating) [8], and electron cyclotron resonance plasma etching (aligned SiNTs arrays) [9], wet etching (nanowire arrays) [10], Femtosecond-laser treatment (penguin-like silicon microstructures) [11]. For instance, porous-pyramid structured Si surface, which was prepared by electrochemical etching and texturization, had an average reflectance of about 1.9% (400–800 nm) due to its gradient-index multilayer structure [12]. The Si nanopillars, which were fabricated by dry etching on the SiO₂-covered Si substrate, acquired an ultra-low reflectance of 0.88% (435 nm) on account of its air/Si mixed structure and highly roughened surface [13]. Single-walled carbon nanotube forest, which was synthesized by water-assisted CVD on silicon substrate, obtained the reflectance of 1%–2% (0.2–200 μm), owing to multiple reflection and absorption from the structure. Although such nanostructures are inconvenient, expensive or not environmental to be constructed, these structures, especially the nanoarrays, still have a lot of inspiration for designing the low-reflectivity material.

CuO nanowires have been widely used in many areas such as in catalysts [14], sensors [15,16], electrode material [17,18], memristors [19], since they were synthesized by heating copper substrate in air from Xia et al. [20]. Recently, Fan et al. [21] prepared CuO/Cu infrared antireflection structure which was constructed by microcone arrays with CuO nanowires via ultrafast laser and thermal oxidation process on Cu surface. The material achieved ultralow total reflectance of about 0.6% at the infrared wavelength around 17 μm and kept steadily below 3% over a broad band of 14–18 μm. On the basis of the previous experience of the solar selective absorber [22], in this work, the ultra-low reflection material of CuO/Cu in UV–vis range is successfully achieved, via designing the ultra-thick and vertically aligned CuO nanowire array. The above array is to be constructed by ultralong CuO nanowires using thermal oxidation method [20]. The experimental process not only does not require any template, corrodent, catalyst, but also does not need ultrafast laser method, etching measure, and electrochemical technique. Even the copper sheet does not need chemical polishing which was previously described by other researchers [23,24]. In this work, the CuO nanowire arrays with different density and thickness are received by varying the reaction temperature and growth time, accordingly their reflectance vary from 0.078% to 5.31%. The array of sample is so thick and dense that the light can be multiply reflected and absorbed while propagates deep into interspace of the nanowires [2, 25], leading to an excellent light trapping. Moreover, the method is facile, low-cost, non-toxic and easy for large-scale industrial production. Herein, the CuO nanowire array represents a new-family of ultra-low reflection material in UV–vis range. It will have a good prospect in harvesting solar energy and improving the sensitivity of optical instruments efficiently.

2. Experimental details

2.1. Preparation

CuO nanowires were synthesized by using the thermal oxidation method [20]. Copper sheets (0.3 mm thick) were used as substrates. They were cut into standard sizes of 3 cm × 5 cm. As for film preparation, the Cu sheets were wiped with alcohol swabs and were not subjected to either chemical or mechanical polishing at first. Then they were placed inside an electric box furnace. The oxidation was carried out at 410 °C and 450 °C in air, respectively.

2.2. Characterization method

X-ray diffraction (XRD) data were collected by a Rigaku D/Max 2550 diffractometer with a monochromator using CuK_α radiation ($\lambda = 1.5418 \text{ \AA}$), which was operated at 50 kV and 200 mA at a scanning rate of 6° min^{-1} in the 2θ range of 30–70° to identify the crystal structures of the films. The EDX, cross sections and morphologies of the samples were examined using field emission scanning electron microscopy (SEM) on a Helios NanoLab 600 I from FEI Company. EDX results for each point of the film were measured for 6 times, and the average intensity was counted. Transmission electron microscope (TEM) were measured using a Tecnai G2 S-Twin F20 with 200 kV accelerating voltage of electron beam. Reflectance with normal incident light in the wavelength interval 0.2–0.7 μm were measured by a Perkin-Elmer Lambda 950 UV/vis/NIR double beam spectrophotometer equipped with an integrating sphere (150 mm).

3. Results and discussion

3.1. TEM results

Fig. 1a shows the TEM image of an individual nanowire whose middle is divided by a twin plane along the longitudinal axis. Fig. 1b displays a high-resolution TEM image, further confirming the bicrystallinity of this nanowire (The lattice fringes in the center are not very clear). Each side of this wire is a single crystal with a well-defined fringe space pattern. The interplanar spacings for each side are 2.51 and 2.33 Å, respectively. These two values correspond well with the spacings calculated for $\{\bar{1}11\}$ and $\{111\}$ planes in monoclinic CuO (cell = $4.69 \text{ \AA} \times 3.43 \text{ \AA} \times 5.13 \text{ \AA}$, $\beta = 99.55^\circ$) [20,26–28]. Fig. 1c shows a diffraction pattern which would be typically observed when the electron beam is focused on an individual nanowire along the $[110]$ direction. The mirror image relationship between the two sets of diffraction spots confirms the formation of a bicrystallinity structure within each nanowire.

3.2. XRD results

Figs. 2 and 3 show the XRD patterns of the samples (a–l) after oxidation at 410 °C and 450 °C for 2 h, 5 h, 10 h, 1 d, 4 d, 7 d, respectively. The XRD results show that the monoclinic CuO is the main oxidation product in each sample, with some Cu₂O after the oxidation in the air [20, 28]. With the increasing of the reaction time at 410 °C or 450 °C from sample a to sample l, the peaks of Cu become weaker, while the $(\bar{2}02)$, (202) , $(\bar{3}11)$ and (220) planes gradually become stronger [29]. The XRD patterns also reveal that the growth planes of the above samples are mostly along the $(\bar{1}11)$ and (111) planes, which are in agreement with the TEM results. Especially, the samples (e, f, k, l) represent the strong peaks on the $(\bar{1}11)$ and (111) planes in virtue of their long nanowires and thick array. The apparent orientation growth along the $[\bar{1}11]$ and $[111]$ planes contributes to forming vertical nanowire arrays.

3.3. EDS results

The cross-sectional SEM image of CuO nanowire array was analyzed by EDS analysis at three points (a: 2.7 μm underneath the nanowire bottom surface, b: 0.6 μm underneath the nanowire bottom surface, c: nanowires at 2.2 μm above the nanowire bottom surface) (Fig. 4). The EDS analysis of the point a displays ~2/1 (Cu/O) atomic ratio which matches with Cu₂O phase (Fig. 4a) [30], while the point b (Fig. 4b) shows ~1/1 (Cu/O) atomic ratio which is corresponding to CuO phase. The point c (Fig. 4c), indicates that the composition of nanowires themselves is ~1/1 (Cu/O) atomic ratio which is in accordance with CuO phase as identified by TEM and XRD results. According to the above results, we conclude that the nanowire arrays are all composed of CuO phase. The upper portion of the bottom oxide layer is also constituted

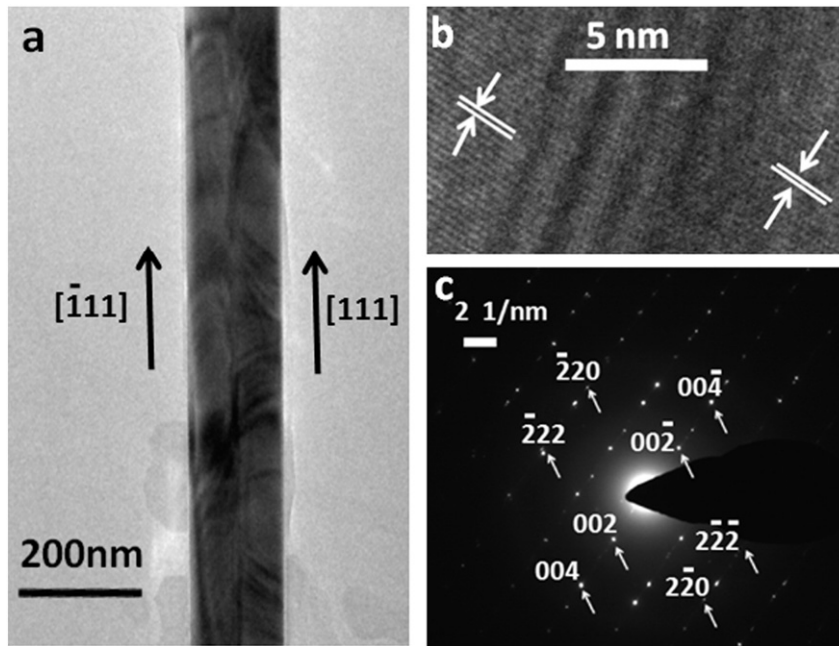


Fig. 1. TEM images of an individual CuO nanowire.

by CuO, while the root portion of the bottom oxide layer contains Cu₂O phase. The vapor-solid (VS) mechanism seems to be responsible for above results [20]. When copper sheet is oxidized in air, the major product is Cu₂O at first. CuO is synthesized through a second step of Cu₂O oxidation. Thus, Cu₂O serves as a precursor to CuO. In this experiment, the reflectance behavior of sample is mostly dominated by the CuO phase, especially the CuO nanowire array.

3.4. Morphology of the samples

Fig. 5 shows the surface SEM images of samples (a–l) prepared at 410 °C and 450 °C for 2 h, 5 h, 10 h, 1 d, 4 d, 7 d, respectively. The gray parts of samples (a, b, c, d, j), which have grown less nanowires on their surface, are also showed (Supporting information, Fig. S1.). The CuO nanowires of sample a, with the diameters between 65 nm–210 nm, are just beginning to come up as the growing time is so short.

When the heating time extends, the nanowires of the samples grow longer and larger. While the copper sheets are heated beyond 4d, the nanowires have diameters of about 78 nm–280 nm, while the top surfaces of their arrays show sparse and deep. As for samples (g–l) heated at 450 °C, the CuO nanowires of sample g are the densest among all these samples and their diameters are only near 45 nm–150 nm. With the extending of heating time, the nanowires, from sample h to sample l, turn to be sparser and larger in diameters gradually, with the diameters varying from 65 nm–200 nm to 70 nm–247 nm. Especially, the array tops of sample k and l seem to be deep pointing to long length of their CuO nanowires. The arrangement of the CuO nanowires which mostly grow along the $\bar{1}11$ and 111 , has a great effect on the optical properties of samples. The deeper and denser nanowire array, brings about the more interaction between the light and CuO nanowire, leading to trap more light and obtain lower reflectivity in the UV–vis region.

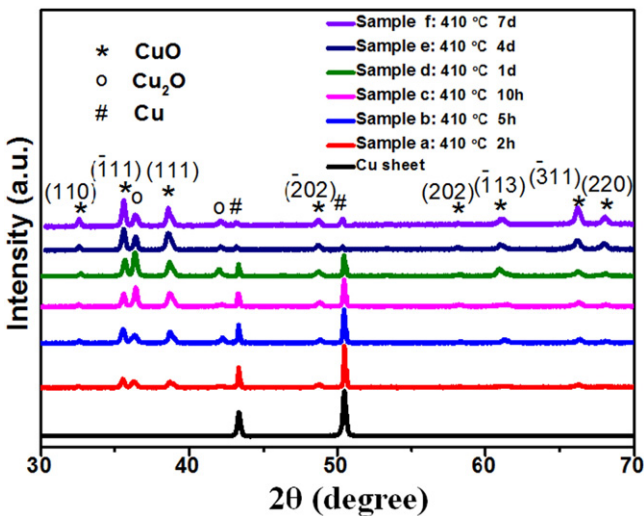


Fig. 2. XRD patterns of Cu substrate (black), sample a (red), sample b (blue), sample c (pink), sample d (green), sample e (mazarine) and sample f (purple).

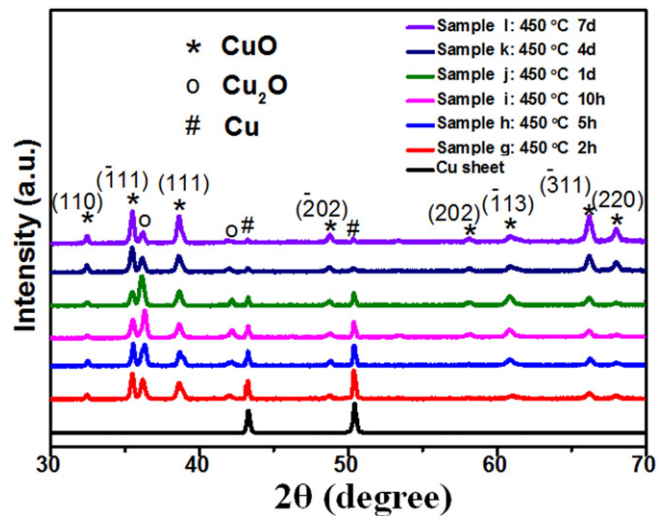


Fig. 3. XRD patterns of Cu substrate (black), sample g (red), sample h (blue), sample i (pink), sample j (green), sample k (mazarine) and sample l (purple).

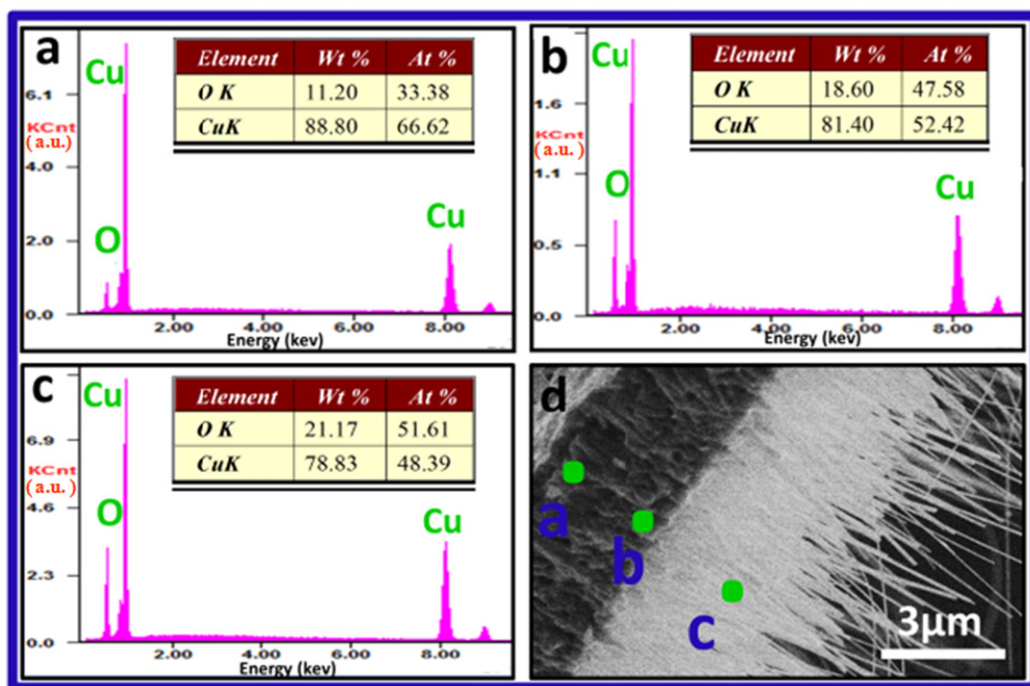


Fig. 4. EDS analysis of CuO nanowire array depending on three positions from cross-sectional SEM image of sample g (a: 2.7 μm underneath nanowire bottom surface, b: 0.6 μm underneath the nanowire bottom surface, c: nanowires at 2.2 μm above the nanowire bottom surface).

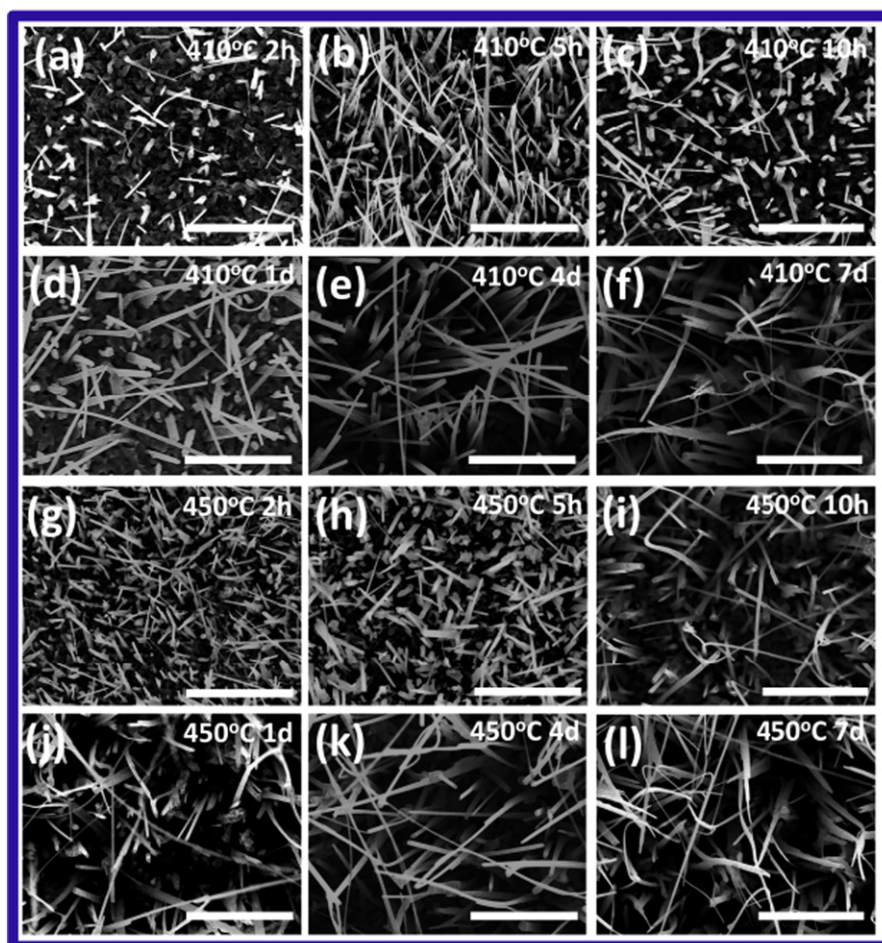


Fig. 5. Surface SEM images of samples (a–f) and (g–l), prepared at 410 °C and 450 °C in air for 2 h, 5 h, 10 h, 1 d, 4 d, 7 d, respectively. Scale bar equals 4 μm, respectively.

3.5. Cross-sections of the samples

Fig. 6 shows the cross sections of samples (a–l) prepared at 410 °C and 450 °C for 2 h, 5 h, 10 h, 1 d, 4 d, 7 d, respectively. The above figure is corresponding with the surface SEM in Fig. 5. The nanowires, most of whom have tilt angles of 0–30°, are nearly perpendicular to the bottom. Their average thicknesses are showed in Table 1. After the sample is heated at 410 °C for 2 h, the CuO nanowires of sample a are starting growing up and their length are relatively short. As for Sample b, its nanowires grow longer and denser. Then, with the heating time extending from 10 h to 1 d, the nanowires become sparse, while only some nanowires come to be longer. With the prolonging of heating time, the arrays of sample e and f turn to be very thick. As for samples heated at 450 °C, the array of sample g is very dense. Similarly, with the extending of the heating time, there's not enough time for a majority of nanowires (from sample h to j) to grow. Therefore, the arrays of those samples are sparse. While the heating time prolongs to 4 d or 7 d, the CuO nanowire arrays of sample k and l turn to be very thick. Their longest nanowires reach to nearly 58.1 μm and 78.8 μm, respectively, which are longer than that of sample e and f. The vertically thick CuO nanowire array plays pivotal role in acquiring ultra-low reflection, owing to that it provides more interaction between the CuO nanowire and light along the micro-interspace which is approximately perpendicular to the substrate. In addition, the different parts of array have different density of nanowires, namely the nanowires come to be denser from the top to the bottom, resulting in gradual changing of refraction index, which is beneficial for trapping light.

Table 1

The average thickness and reflectance of the samples prepared at different conditions.

Sample number	Preparation conditions	Average thickness (μm)	Average reflectance
Samples a	410 °C, 2 h	2.1 μm	4.58%
Samples b	410 °C, 5 h	4.1 μm	3.01%
Samples c	410 °C, 10 h	4.5 μm	3.58%
Samples d	410 °C, 1 d	3.7 μm	5.31%
Samples e	410 °C, 4 d	20.4 μm	0.63%
Samples f	410 °C, 7 d	28.9 μm	0.35%
Samples g	450 °C, 2 h	6.0 μm	0.82%
Samples h	450 °C, 5 h	5.2 μm	1.01%
Samples i	450 °C, 10 h	6.1 μm	1.29%
Samples j	450 °C, 1 d	5.3 μm	2.30%
Samples k	450 °C, 4 d	28.1 μm	0.34%
Samples l	450 °C, 7 d	40.3 μm	0.078%

3.6. Reflectance results

Reflectance spectra (Figs. 7 and 8) are measured with normal incident light at room temperature in UV–vis spectrum range (200–700 nm), respectively. The photographs of samples (a–l) are shown in their insets. The average reflectance of above samples are calculated and showed in Table 1. However, the average reflectance of Cu substrate is only 44.64% (Supporting information, Fig. S2). The reflectance of the gray parts for samples (a–d) are all exceeding 6.5% (Supporting information, Fig. S3). The surface colors of above samples change due to their different reflection ability. Sample f, k and l, especially the sample

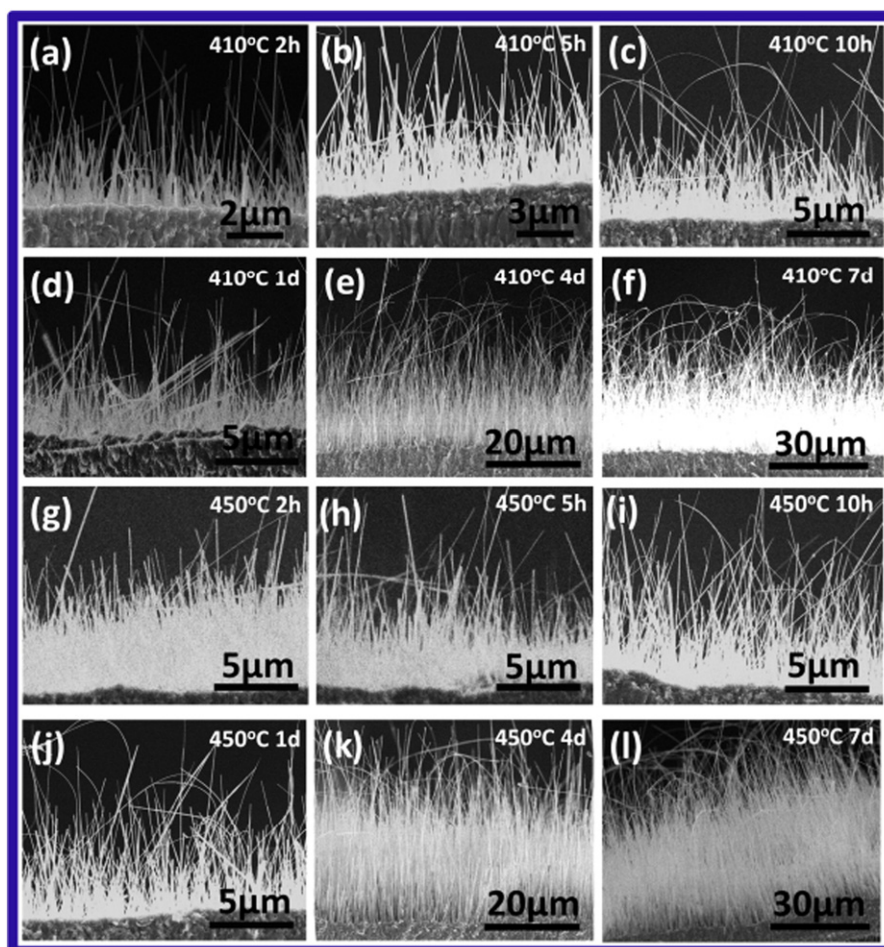


Fig. 6. Cross-sectional SEM images of samples (a–f) and (g–l), prepared at 410 °C and 450 °C in air for 2 h, 5 h, 10 h, 1 d, 4 d, 7 d, respectively.

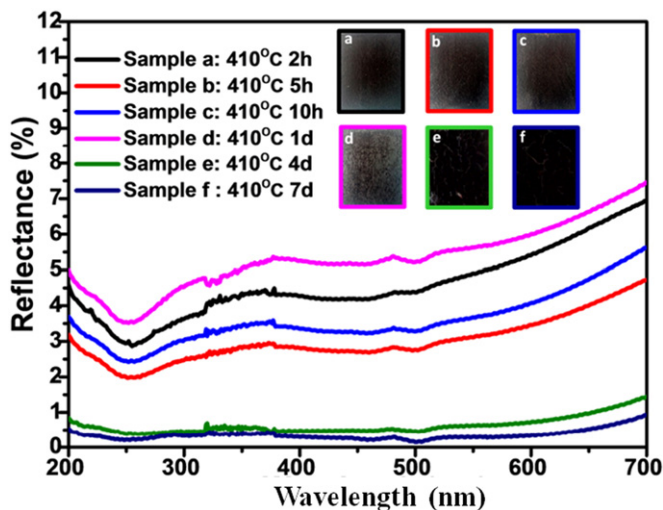


Fig. 7. Reflectance of sample a (black), sample b (red), sample c (blue), sample d (pink), sample e (green), sample f (mazarine). Insets (a–f) are their photos, respectively.

l, shows dark black in appearance and implies excellent ultra-low reflection property, as a result of their thick and dense CuO nanowire arrays. It is found that the reflectance of samples is greatly affected by the CuO nanowire arrays on surface. Density and thickness of the nanowire array, especially the thickness, are essential to obtain this property.

To study the light suppression of CuO nanowire arrays in different UV–vis spectral wavelength ranges, the various arithmetical average reflectance of samples (a–l) are concluded and showed in Fig. 9 and Fig. 10. Even from the perspective of the entire spectrum range from 200 nm to 700 nm, the broadband low-reflection properties maintain effectiveness. As for samples heated at 410 °C for less than 4 d, owing to that the nanowires have not grown long and dense all round the samples, therefore the resultant average reflectance of above samples (Fig. 9a) is the hybrid performance of the CuO nanowire arrays and the gray parts which have less nanowires on surface. Hence the change trends of the average reflectance for above samples at different wavelength bands are influenced by those of the gray parts (Supporting information, Fig. S4). Besides, sample e is also partially affected by

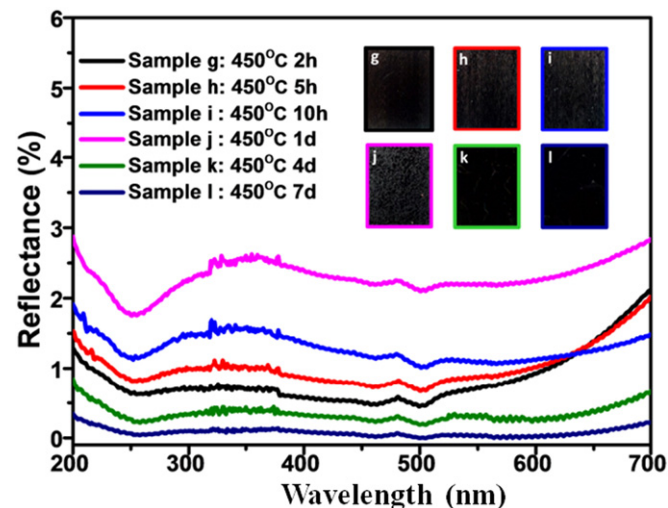


Fig. 8. Reflectance of sample g (black), sample h (red), sample i (blue), sample j (pink), sample k (green), sample l (mazarine). Insets (g–l) are their photos, respectively.

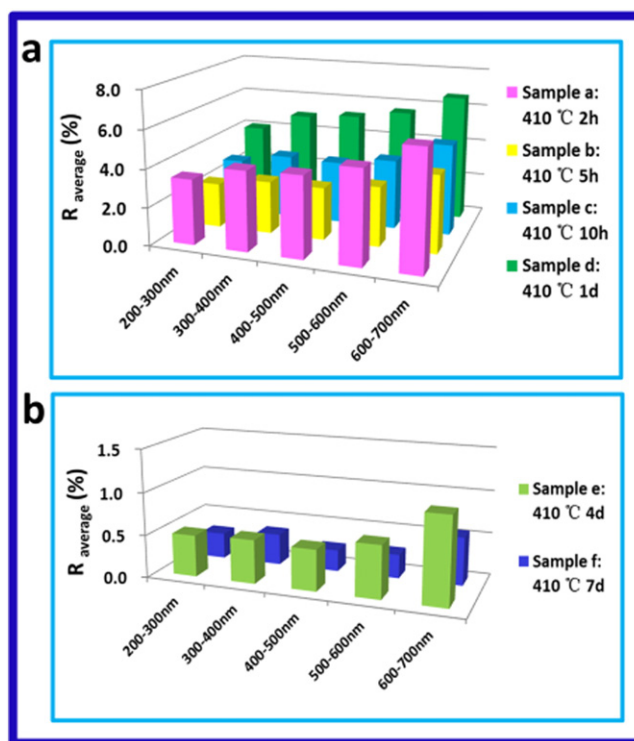


Fig. 9. The average reflectance in different wavelength ranges of samples (a–f) prepared at 410 °C in air for 2 h, 5 h, 10 h, 1 d, 4 d, 7 d, respectively.

exposed copper substrate as its surface CuO nanowire array has partly been ruptured (Fig. 9b; Supporting information, Fig. S5). Based on sample f to sample l (Fig. 10), especially the sample f, k and l, accordingly it can be found that the CuO nanowire arrays have more influence on

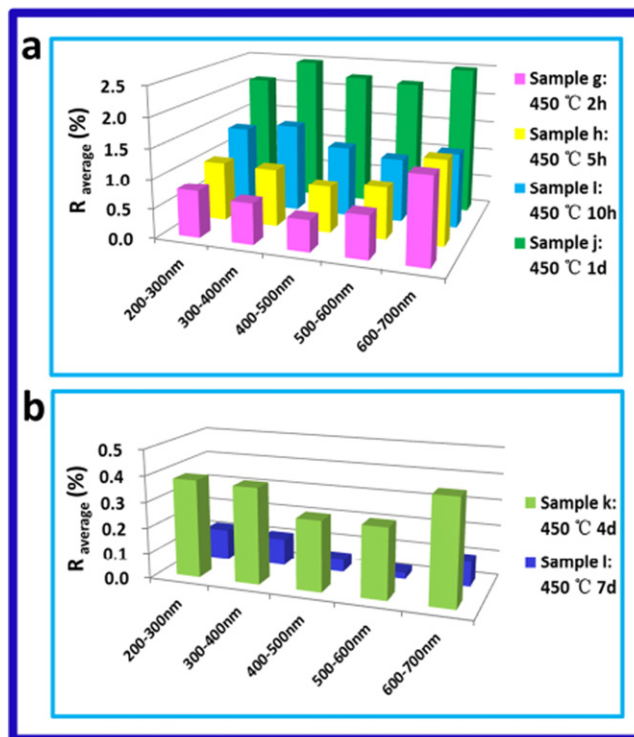


Fig. 10. The average reflectance in different wavelength ranges of samples (g–l) prepared at 450 °C in air for 2 h, 5 h, 10 h, 1 d, 4 d, 7 d, respectively.

suppressing the reflection within the 400–500 nm and 500 nm–600 nm ranges, with the lowest values of 0.0478% and 0.0235% being reached from sample I within above ranges. This indicates that nearly 99.95% of the surface reflection has been successfully eliminated and trapped via the vertically aligned CuO nanowire array.

The ultra-low reflectivity of CuO nanowire arrays come from the following two reasons (Fig. 11):

1, As shown in the Fig. 6, CuO nanowires are almost vertically aligned, with tilt angles of 0–45° (most of the nanowires with tilt angles of 0–30°). Consequently, when the majority of the light proceeds into the nanowire array, interaction between the light and CuO nanowire will happen (Fig. 11a). For each interaction, one part of light will be reflected on the surface, while the other part will be absorbed, due to the fact that CuO is a good absorber [23,24,31] over the UV–Vis spectrum range with the bandgap energy (1.2 eV to 2.1 eV). As the light propagates further into the deep interspace formed by nanowires, it is continually interacting with the nanowire and absorbed by the nanowire in succession. This interaction repeats until the attenuated light is almost completely absorbed by the nanowires [2,25]. Therefore, the thicker and denser the CuO nanowire array is, the more probably the light will be interacting and absorbed, at last the excellent suppression of light reflection will be acquired.

2, The gradient refractive index of the array is also in favor of the low reflection. CuO nanowire array can be treated as an effective medium which is filled with air as shown in Fig. 11b. The array can be divided into N layer. The n_{air} and n_s represent the refractive indices of air and substrate, respectively. The n_i represents the refractive index of the i th layer in the structure [32], with $n_{\text{air}} < n_1 < n_2 < \dots < n_i < \dots < n_{N-2} < n_{N-1} < n_N < n_s$ ($n_{\text{air}} = 1$). The refractive index of the i th layer is estimated by,

$$n_i = f_i n_{\text{air}} + (1 - f_i) n_{\text{CuO}}$$

where f_i is a filling factor of air [21]. From the surface of array to the bottom, the filling factor gradually reduces to near zero, accordingly the refraction index of each layer is gradually increasing. The relationship

between the reflectance and the refraction index can be described by the following formula [12,33]:

$$R = (n_{i+1} - n_i)^2 / (n_{i+1} + n_i)^2$$

where n_i and n_{i+1} represent the refractive indices of two adjacent layers, respectively. It can be deduced that, the less value the $|n_{i+1} - n_i|$ has, then the lower reflectance the array will obtain. As for the thicker CuO nanowire array, the refractive index of whole array changes more slowly from the top to the bottom, then the difference of refractive indices for the two adjacent layers are smaller, easily leading to lower reflectivity.

4. Conclusion

In summary, the ultra-low reflection material of CuO/Cu in UV–vis range is successfully designed and achieved in our work, via orderly growing ultralong CuO nanowires on copper sheet to construct the ultra-thick and vertically aligned array. Our experimental process is convenient, low-cost, pollution-free and suitable for bulk production. It unnecessarily requires any template, corrodent, catalyst, ultrafast laser method, etching measure, or electrochemical technique. Besides, the pretreatment of the copper sheet is also very simple. In this experiment, the density and thickness of CuO nanowire array can be tuned by varying the reaction temperature and growth time. The ultra-low reflectivity of CuO nanowire arrays is due to the following reasons: Firstly, the array is so thick and dense that the light can be multiply reflected and absorbed when it propagates deeply into the interspace of the nanowires, leading to an excellent light trapping. Secondly, the array can be regarded as air-filled gradient refractive index medium, which is also in favor of the low reflection. In this experiment, the nanowire array with the lowest reflectivity and dark black appearance among above samples is obtained at 450 °C for 7 d, with average array thickness of about 40.5 μm and average reflectance of 0.078% in 200–700 nm region. Herein, the CuO nanowire array represents a new-family of ultra-low reflection material in UV–vis range. It will have a good

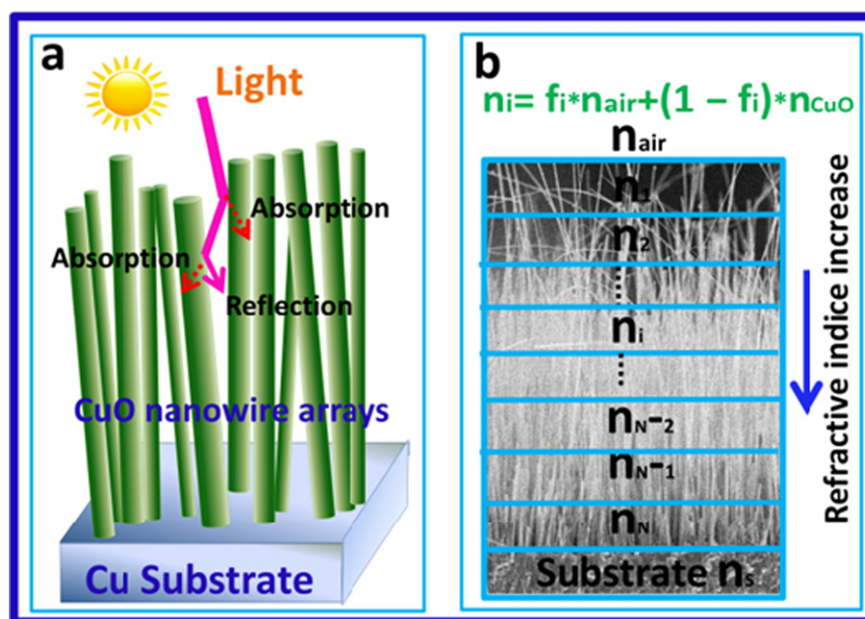


Fig. 11. Schematic diagrams illustrating the ultra-low reflectivity of CuO nanowire arrays: 1. The array is so thick and dense that the light can be multiply reflected and absorbed while propagates deep into the interspace of the nanowires, leading to an excellent light trapping. 2. The array can be regarded as air-filled gradient refractive index medium, which is also in favor of the low reflection.

industrial-production prospect in harvesting solar energy, and improving the sensitivity of optical instruments by blackening the inner-wall of drawtube or sample compartment.

Acknowledgements

This work was supported by the National Natural Science Foundation of China (grants 21427802, 21131002).

Appendix A. Supplementary data

Supplementary data to this article can be found online at <http://dx.doi.org/10.1016/j.matdes.2016.10.029>.

References

- [1] A. Cao, X. Zhang, C. Xu, B. Wei, D. Wu, Tandem structure of aligned carbon nanotubes on Au and its solar thermal absorption, *Sol. Energy Mater. Sol. Cells* 70 (2002) 481–486.
- [2] K. Mizuno, J. Ishii, H. Kishida, Y. Hayamizu, S. Yasuda, D.N. Futaba, M. Yumura, K. Hata, A black body absorber from vertically aligned single-walled carbon nanotubes, *Proc. Natl. Acad. Sci. U. S. A.* 106 (2009) 6044–6047.
- [3] M. Ibn-Elhaj, M. Schadt, Optical polymer thin films with isotropic and anisotropic nano-corrugated surface topologies, *Nature* 410 (2001) 796–799.
- [4] A. Divochiy, F. Marsili, D. Bitauld, A. Gaggero, R. Leoni, F. Mattioli, A. Korneev, V. Seleznev, N. Kurova, O. Minaeva, Superconducting nanowire photon-number-resolving detector at telecommunication wavelengths, *Nat. Photonics* 2 (2008) 302–306.
- [5] N. Fox, Trap detectors and their properties, *Metrologia* 28 (1991) 197.
- [6] R.J. Brown, P.J. Brewer, M.J. Milton, The physical and chemical properties of electrodeless nickel-phosphorus alloys and low reflectance nickel-phosphorus black surfaces, *J. Mater. Chem.* 12 (2002) 2749–2754.
- [7] X. Li, X. Yu, Y. Han, Polymer thin films for antireflection coatings, *J. Mater. Chem. C* 1 (2013) 2266–2285.
- [8] A. Shashikala, A. Sharma, D. Bhandari, Solar selective black nickel-cobalt coatings on aluminum alloys, *Sol. Energy Mater. Sol. Cells* 91 (2007) 629–635.
- [9] Y.-F. Huang, S. Chattopadhyay, Y.-J. Jen, C.-Y. Peng, T.-A. Liu, Y.-K. Hsu, C.-L. Pan, H.-C. Lo, C.-H. Hsu, Y.-H. Chang, Improved broadband and quasi-omnidirectional anti-reflection properties with biomimetic silicon nanostructures, *Nat. Nanotechnol.* 2 (2007) 770–774.
- [10] H.-C. Chang, K.-Y. Lai, Y.-A. Dai, H.-H. Wang, C.-A. Lin, J.-H. He, Nanowire arrays with controlled structure profiles for maximizing optical collection efficiency, *Energy Environ. Sci.* 4 (2011) 2863–2869.
- [11] X. Liu, P.R. Coxon, M. Peters, B. Hoex, J.M. Cole, D.J. Fray, Black silicon: fabrication methods, properties and solar energy applications, *Energy Environ. Sci.* 7 (2014) 3223–3263.
- [12] H. Lv, H. Shen, Y. Jiang, C. Gao, H. Zhao, J. Yuan, Porous-pyramids structured silicon surface with low reflectance over a broad band by electrochemical etching, *Appl. Surf. Sci.* 258 (2012) 5451–5454.
- [13] Y.-H. Pai, F.-S. Meng, C.-J. Lin, H.-C. Kuo, S.-H. Hsu, Y.-C. Chang, G.-R. Lin, Aspect-ratio-dependent ultra-low reflection and luminescence of dry-etched Si nanopillars on Si substrate, *Nanotechnology* 20 (2009) 035303.
- [14] Y. Feng, X. Zheng, Plasma-enhanced catalytic CuO nanowires for CO oxidation, *Nano Lett.* 10 (2010) 4762–4766.
- [15] J. Chen, K. Wang, L. Hartman, W. Zhou, H₂S detection by vertically aligned CuO nanowire array sensors, *J. Phys. Chem. C* 112 (2008) 16017–16021.
- [16] F. Yang, J. Guo, M. Liu, S. Yu, N. Yan, J. Li, Z. Guo, Design and understanding of a high-performance gas sensing material based on copper oxide nanowires exfoliated from a copper mesh substrate, *J. Mater. Chem. A* 3 (2015) 20477–20481.
- [17] L. Chen, N. Lu, C. Xu, H. Yu, T. Wang, Electrochemical performance of polycrystalline CuO nanowires as anode material for Li ion batteries, *Electrochim. Acta* 54 (2009) 4198–4201.
- [18] L. Ji, Z. Lin, M. Alcoutlabi, X. Zhang, Recent developments in nanostructured anode materials for rechargeable lithium-ion batteries, *Energy Environ. Sci.* 4 (2011) 2682–2699.
- [19] Z. Fan, X. Fan, A. Li, L. Dong, In situ forming, characterization, and transduction of nanowire memristors, *Nanoscale* 5 (2013) 12310–12315.
- [20] X. Jiang, T. Herricks, Y. Xia, CuO nanowires can be synthesized by heating copper substrates in air, *Nano Lett.* 2 (2002) 1333–1338.
- [21] P. Fan, B. Bai, J. Long, D. Jiang, G. Jin, H. Zhang, M. Zhong, Broadband high-performance infrared antireflection nanowires facilely grown on ultrafast laser structured Cu surface, *Nano Lett.* 15 (2015) 5988–5994.
- [22] X. Wang, X. Wu, L. Yuan, C. Zhou, Y. Wang, K. Huang, S. Feng, Solar selective absorbers with foamed nanostructure prepared by hydrothermal method on stainless steel, *Sol. Energy Mater. Sol. Cells* 146 (2016) 99–106.
- [23] X. Xiao, L. Miao, G. Xu, L. Lu, Z. Su, N. Wang, S. Tanemura, A facile process to prepare copper oxide thin films as solar selective absorbers, *Appl. Surf. Sci.* 257 (2011) 10729–10736.
- [24] S. Karthick Kumar, S. Suresh, S. Murugesan, S.P. Raj, CuO thin films made of nanofibers for solar selective absorber applications, *Sol. Energy* 94 (2013) 299–304.
- [25] S. Thiyagu, B.P. Devi, Z. Pei, Fabrication of large area high density, ultra-low reflection silicon nanowire arrays for efficient solar cell applications, *Nano Res.* 4 (2011) 1136–1143.
- [26] K. Zhang, C. Rossi, C. Tenailleau, P. Alphonse, J.-Y. Chane-Ching, Synthesis of large-area and aligned copper oxide nanowires from copper thin film on silicon substrate, *Nanotechnology* 18 (2007) 275607.
- [27] D. Zappa, E. Comini, R. Zamani, J. Arbiol, J.R. Morante, G. Sberveglieri, Preparation of copper oxide nanowire-based conductometric chemical sensors, *Sensors Actuators B Chem.* 182 (2013) 7–15.
- [28] J.T. Chen, F. Zhang, J. Wang, G.A. Zhang, B.B. Miao, X.Y. Fan, D. Yan, P.X. Yan, CuO nanowires synthesized by thermal oxidation route, *J. Alloys Compd.* 454 (2008) 268–273.
- [29] Y.-S. Kim, I.-S. Hwang, S.-J. Kim, C.-Y. Lee, J.-H. Lee, CuO nanowire gas sensors for air quality control in automotive cabin, *Sensors Actuators B Chem.* 135 (2008) 298–303.
- [30] T.K. Kim, B. VanSaders, J. Moon, T. Kim, C.-H. Liu, J. Khamwannah, D. Chun, D. Choi, A. Kargar, R. Chen, Tandem structured spectrally selective coating layer of copper oxide nanowires combined with cobalt oxide nanoparticles, *Nano Energy* 11 (2015) 247–259.
- [31] R. Shabu, A.M.E. Raj, C. Sanjeeviraja, C. Ravidhas, Assessment of CuO thin films for its suitability as window absorbing layer in solar cell fabrications, *Mater. Res. Bull.* 68 (2015) 1–8.
- [32] L. Ma, Y. Zhou, N. Jiang, X. Lu, J. Shao, W. Lu, J. Ge, X. Ding, X. Hou, Wide-band “black silicon” based on porous silicon, *Appl. Phys. Lett.* 88 (2006) 171907.
- [33] B. Karlsson, C.G. Ribbing, A. Roos, E. Valkonen, T. Karlsson, Optical properties of some metal oxides in solar absorbers, *Phys. Scr.* 25 (1982) 826.